Biochemical and Biophysical Research Communications 590 (2022) 97–102

Contents lists available at ScienceDirect

Biochemical and Biophysical Research Communications

journal homepage: www.elsevier.com/locate/ybbrc

Pluripotency state of mouse ES cells determines their contribution to self-organized layer formation by mesh closure on microstructured adhesion-limiting substrates

Yuta Ando [a, b], Kennedy Omondi Okeyo [a, b, c, *], Taiji Adachi [a, b, c]

[a] Department of Micro Engineering, Graduate School of Engineering, Kyoto University, Kyoto Daigaku-katsura, Nishikyo-ku, Kyoto, 615-8530, Japan
[b] Institute for Frontier Life and Medical Sciences, Kyoto University, 53 Shogoin Kawahara-cho, Sakyo-ku, Kyoto, 606-8507, Japan
[c] Division of Systemic Life Science, Graduate School of Biostudies, Kyoto University, Yoshida-Konoecho, Sakyo-ku, Kyoto, 606-8501, Japan

ARTICLE INFO

Article history:
Received 7 December 2021
Accepted 18 December 2021
Available online 21 December 2021

Keywords:
Embryonic stem cells
Pluripotency
Naïve state
Ground state
Layer formation
Mesh substrates

ABSTRACT

Assembly of pluripotent stem cells to initiate self-organized tissue formation on engineered scaffolds is an important process in stem cell engineering. Pluripotent stem cells are known to exist in diverse pluripotency states, with heterogeneous subpopulations exhibiting differential gene expression levels, but how such diverse pluripotency states orchestrate tissue formation is still an unrevealed question. In this study, using microstructured adhesion-limiting substrates, we aimed to clarify the contribution to self-organized layer formation by mouse embryonic stem cells in different pluripotency states: ground and naïve state. We found that while ground state cells as well as sorted REX1-high expression cells formed discontinuous cell layers with limited lateral spread, naïve state cells could successfully self-organize to form a continuous layer by progressive mesh closure within 3 days. Using sequential immunofluorescence microscopy to examine the mesh closure process, we found that KRT8+ cells were particularly localized around unfilled holes, occasionally bridging the holes in a manner suggestive of their role in the closure process. These results highlight that compared with ground state cells, naïve state cells possess a higher capability to contribute to self-organized layer formation by mesh closure. Thus, this study provides insights with implications for the application of stem cells in scaffold-based tissue engineering.

1. Introduction

Pluripotent stem cells are attractive cell sources for self-organized tissue formation due to their unique differentiation capacity, as well as their ability to mimic embryogenic processes [1]. For instance, these cells hold the promise for achieving engineered tissues such as stem cell sheets for application in regenerative medicine [2]. Microengineered scaffolds are increasingly becoming important in stem cell engineering because they enable the modulation of the adhesion microenvironment which in turn enhance cell-cell interaction to initiate robust tissue formation [3,4]. Thus, engineered substrates can be harnessed to tune the self-organization progress of pluripotent stem cells to induce tissue formation by controlling the assembly of cells. Although self-organization property has been the subject of numerous studies, how stem cell pluripotency state influences this process remains largely unclear. Clarifying the contribution of stem cells in different pluripotency states to self-organized layer formation would enable better control of the tissue formation process using engineered scaffolds, with important implications for application of stem cells in tissue engineering.

It is generally known that mouse embryonic stem cells (mESCs) exhibit two major pluripotency states: naïve and ground states. The naïve state mESCs are maintained by supplementing the culture medium with leukemia inhibitory factor (LIF) [5], and are known to be a heterogeneous population exhibiting a wide variation in gene expression [6,7]. On the other hand, the ground state mESCs are a more homogeneous population obtained by chemical induction using dual inhibition (2i) with mitogen-activated extracellular signal-regulated kinase (MEK) and glycogen synthase kinase 3 (GSK3) [8]. The differential gene expression patterns between

* Corresponding author. Institute for Frontier Life and Medical Sciences, Kyoto University, 53 Shogoin Kawahara-cho, Sakyo-ku, Kyoto, 606-8507, Japan.
E-mail address: okeyo@infront.kyoto-u.ac.jp (K.O. Okeyo).

https://doi.org/10.1016/j.bbrc.2021.12.066

ground and naïve state mESCs have been made clearer by recent advances in single-cell analysis [9–12]. For instance, the ground state mESCs uniformly express REX1 but the naïve state mESCs exhibit a mosaic-in-colony expression [6,7,13]. In addition, the heterogeneous gene expression pattern in pluripotent stem cell subpopulations has been suggested as an important driver of subsequent cell fate decision and symmetry breaking [14]. However, how mESCs in the different pluripotency states (ground and naïve state) contribute to the layer formation remains largely unexplored.

In the present study, using adhesion-limiting mesh substrates, we aimed to clarify the contribution of mESCs in ground and naïve states to self-organized layer formation. The mesh substrates have been previously demonstrated to drive self-organization into cell layers without biochemical inductions [15]. For comparison, we evaluated both ground and naïve state mESCs, based on REX1, OCT3/4 and KRT8 (cytokeratin 8) expressions. OCT3/4 is one of the major transcription factors which is known to be essential for pluripotency maintenance [5]. KRT8 has been identified as a marker of a subpopulation of naïve state mESCs nearly exiting pluripotency [7,10]. Based on the morphology of the self-organized cell layers, we show that ground and naïve state mESCs exhibit differential potential in their contribution to self-organized layer formation by progressive mesh closure on the adhesion-limiting mesh substrates.

2. Materials and methods

2.1. Cell culture

In this study, we used mESC line OLV2-1 (Riken Cell Bank) expressing knocked-in OCT3/4-linker-Venus vector, and OCRG9 (Riken Cell Bank) expressing a knocked-in REX1-EGFP-IB and OCT3/4-linker-ECFP vectors [6]. Both mESCs were maintained with G-MEM (Wako) with 10% fetal bovine serum (FBS; Sigma-Aldrich), 1 mM sodium pyruvate (Wako), 1% MEM non-essential amino acids (Wako), 0.1 mM 2-mercaptoethanol (Wako) and 1000 units/mL leukemia inhibitory factor (LIF; Wako). For 2i + LIF culture, 3 μM CHIR99021 (Wako) and 1 μM PD0325901 (Wako) were added to the culture medium. The cells were cultured at 37 °C and 5% CO_2 on cell culture dishes coated with 0.1% gelatin from porcine skin (gel strength 300, type A; Sigma-Aldrich). For passage, the cells were dissociated by TrypLE Express (Thermo Fisher Scientific) and seeded at 7.0×10^3 cells/cm^2 for 2-day interval passage or 2.6×10^3 cells/cm^2 for 3-day interval passage.

2.2. Cell culture on microstructured mesh substrates

Microstructured mesh substrates were fabricated by photolithography using SU-8 2 (MicroChem), an epoxy-based negative photoresist, as reported previously [15–17]. The fabricated mesh substrate was mounted on a 0.5 mm-thick silicon rubber spacer and placed on a culture dish. mESCs on the microstructured mesh substrates were cultured with the pluripotency maintenance medium with antibiotic antimycotic solution (Sigma-Aldrich). To promote cell attachment, the substrates were coated with a matrix protein (laminin) by incubating them for 1 h at 37 °C with 10 μg/mL solution of laminin-511 E8 fragment (iMatrix-511 silk; Nippi) diluted in phosphate buffered saline (PBS). For cell seeding, cell density was adjusted to $1.0–5.0 \times 10^6$ cells/mL, and 100 μL of the cell suspension was gently added drop-by-drop onto the mesh substrates. Cells were then incubated for 6 h at 37 °C and 5% CO_2 to allow for cell attachment on the mesh lines. The cell-loaded mesh substrates were transferred to a new culture dish in order to discard fallen cells. Finally, fresh culture medium was added and culture continued undisturbed. Day 0 was defined as the start of cell culture on mesh sheets.

2.3. Cell staining and immunofluorescence microscopy

Cells were fixed with 4% paraformaldehyde in PBS and then permeabilized with 0.1% polyethylene glycol mono-p-isooctylphenyl ether (Nacalai Tesque) in PBS. After blocking with 3% bovine serum albumin (Sigma-Aldrich) in PBS, staining reagents diluted in 1% bovine serum albumin in PBS were applied. For immunofluorescence staining, anti-cytokeratin 8 antibody (1:200; ab53280; Abcam) was used as a primary antibody, and F(ab')2-goat anti-rabbit IgG (H + L) cross-adsorbed Alexa Fluor 546 (1:500; A-11071; Thermo Fisher Scientific) or goat anti-rabbit IgG H&L Alexa Fluor 568 (1:500; ab175471; Abcam) was used as a secondary antibody. For staining cell nucleus, 4′,6-diamidino-2-phenylindole (DAPI; 1:500; D1306; Thermo Fisher Scientific) or 7-amino-actinomycin D (7-AAD; 1:50; ab228563; Abcam) was used. For staining the F-actin cytoskeleton, Alexa Flour 647 phalloidin (1:100; A22287; Thermo Fisher Scientific) was used. Immunofluorescence microscopy was performed with FLUOVIEW FV3000 confocal laser scanning microscope (Olympus).

2.4. Image processing and quantitative analyses

Acquired immunofluorescence images were processed, reconstructed and analyzed using Fiji [18]. For quantitative analyses of self-organized layer, first we obtained binarized images of acquired 16-bit stacked confocal images and then calculated the threshold values for each channel. To binarize all the slices with the single threshold value, the threshold was computed by the Otsu's method in “Auto Threshold” plugin of Fiji, based on a histogram of all the slices. Next, the voxels where the layer exist were determined by the both binarized images of nuclei (DAPI or 7-AAD) and F-actin (phalloidin), and then layer thickness $d(x,y)$ was calculated by integrating the number of voxels in each XY position along Z axis. Mesh coverage were determined as the percentage of the nonzero values of $d(x,y)$ over all $d(x,y)$, and mean layer thickness was determined as the average of nonzero values of $d(x,y)$.

2.5. Fluorescence-activated cell sorting

For cell sorting to obtain REX1-high population from naïve state mESCs, dissociated cells from culture dishes were suspended in the culture medium and analyzed using BD FACSMelody cell sorter (BD Biosciences). Manual gating based on forward and side scatter signals was performed to obtain a cell population. First, EGFP positive gate was determined using unlabeled mESCs. Then, REX1-high population was sorted according to REX1-EGFP-high gate which was determined manually. Visualization of the sorted cell population was performed using FlowJo single cell analysis software (BD Biosciences).

3. Results

3.1. Ground and naïve state mouse ES cells demonstrated contrasting layer-forming potential on adhesion-limiting mesh substrates

mESCs under pluripotency maintenance culture are known to exist in different pluripotency states with different expression signatures (Fig. 1A). To determine the layer-forming potential of mESCs at different pluripotency states, we utilized adhesion-limiting mesh substrates [15,16] to assess and compare self-organized layer formation by mESCs converted to ground state versus naïve state mESCs. Conversion from naïve state to ground state was achieved by culturing naïve state mESCs (the default mESC state) on typical culture dishes under 2i + LIF condition for

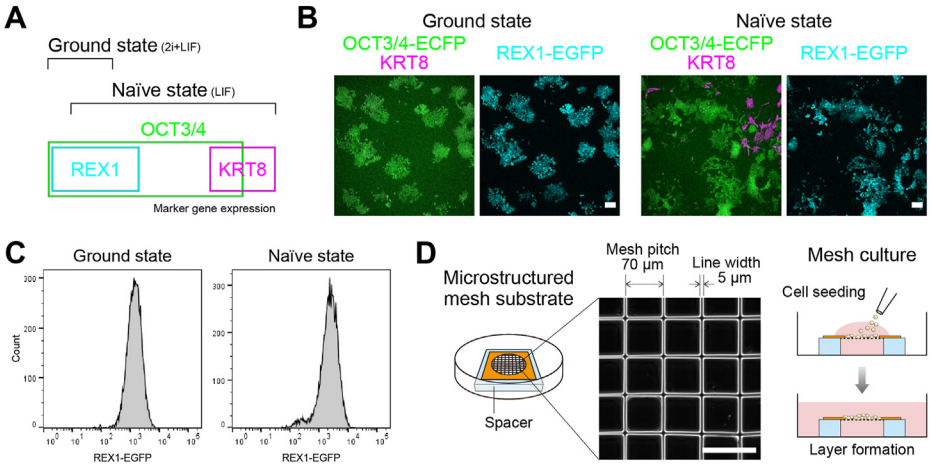

Fig. 1. Experimental setup to induce self-organized layer formation by mESCs in different pluripotency states on microstructured mesh substrates. (A) Schematic illustration of ground and naïve states, and marker gene expressions used in this study. (B) Microscopic images of the ground and naïve state mESCs. (C) REX1 expression of ground and naïve state mESCs cultured on typical culture dishes. (D) Schematic illustration of mesh substrate setup in a suspended position for cell seeding, and the self-organization processes leading to layer formation.

one week, with two passages in between. As confirmed using immunofluorescence microscopy, we succeeded in generating ground state mESCs exhibited global expression of REX1, but KRT8+ cells were not observed (Fig. 1B, left and 1C). In contrast, the naïve state mESCs on dish consisted of two subpopulations: one existing in compact colonies with high OCT3/4 expression (OCT3/4+ cells), and another as scattered single cells with visibly high KRT8 expression (KRT8+ cells) (Fig. 1B, right). Strikingly, KRT8+ cells exhibited expanded shape and were widely scattered around OCT3/4+ clusters, consistent with previous studies [7,19]. Based on these observations as well as past studies [10,13], we confirmed the different expression patterns of REX1 and KRT8 in the ground and naïve state mESCs. In the subsequent experiments, we cultured mESCs and induced them to form continuous cell layers on ~2 μm-thick microstructured mesh substrates (pitch: 70 μm, line width: 5 μm), which were set suspended in the culture medium as shown in Fig. 1D.

We sought to investigate how mESCs in different pluripotency states due to their culture condition would contribute to cell layer formation by mesh closure on the mesh substrate. Ground and naïve state mESCs seeded separately on the mesh substrates for 3 days under 2i + LIF or LIF condition exhibited different mesh filling capability and layer morphologies. Under 2i + LIF condition, ground state cells formed pancake-shaped punctate clusters which predominantly comprised of OCT3/4+ cells but not KRT8+ cells (Fig. 2A, left). But under LIF condition, the ground state cells exhibited slightly increased layer formation potential, and could be seen forming patches of layers covering a slightly larger area of the partially filled mesh substrate than observed under 2i + LIF condition, although many unfilled holes could still be seen at Day 3 (Fig. 2A, right). In contrast, under both 2i + LIF and LIF condition, the naïve state cells could fill the mesh openings sufficiently well, resulting in the formation of a continuous layer by Day 3 (Fig. 2B). To compare the spatial localization OCT3/4+ cells versus KRT8+ cells, we performed confocal microscopy to examine the vertical cross-section of the self-organized cell layer. Intriguingly, we found that KRT8+ cells occupied the upper and lower surfaces of the formed cell layer, sandwiching OCT3/4+ cells in the layer interior (Fig. 2B, vertical cross-sections). Next, for quantitative comparison, we quantified the mesh coverage and mean thickness under each culture condition based on fluorescence images captured by labeling DAPI and phalloidin (Fig. 2C). We found that ground state cells under 2i + LIF condition formed thick layers with limited lateral spread (low coverage and greater mean thickness, 51.4 ± 2.1 μm), as opposed to naïve state cells which formed a continuous cell layer cover over the mesh substrates regardless of the maintenance condition (2i + LIF or LIF), as shown in Fig. 2C. These results suggest that self-organized cell layer formation on the mesh substrates by mesh closure was determined by the pluripotency state before mesh seeding but not the media condition.

3.2. *REX1-high population sorted from naïve state cells formed discontinuous cell layers*

According to previous research [13], naïve state mESCs with high expression of REX1 were reported to exhibit ground state-like features, but with differences in gene expression compared with 2i + LIF-derived ground state mESCs. We therefore sought to determine if REX1-high population sorted from naïve state mESCs would form discontinuous cell layers similar to ground state mESCs. To examine this, we conducted a comparative experiment by sorting REX1-high expressing cell population (Fig. 3A) and examined their layer formation potential on the adhesion-limiting substrates by mesh closure. To specifically obtain ground state-like REX1-high population, sorting was performed by gating for the approximately top 30% of the total naïve state mESCs which exhibited high expression of REX1-EGFP (Fig. 3B, histogram).

When seeded on the mesh substrate under LIF condition, the REX1-high population also formed discontinuous layers with many holes still visible at Day 3 (Fig. 3B), similar to ground state cells. Moreover, whereas OCT3/4 and REX1 were globally expressed on the mesh substrates, KRT8 expression was not observed (Fig. 3B). Quantitative analysis further confirmed incomplete mesh coverage for REX1-high population, although this population did not show significant difference in the mean layer thickness (31.8 ± 7.9 μm) compared with the naïve state cells (Fig. 3C). Collectively, these results showed that REX1-high population was not as efficient as naïve state cells in filling the mesh openings to form a continuous cell layer by mesh closure. These results further illustrated that even within naïve state mESCs, which is a heterogeneous population [6,10,13], the subset with ground state-like property (designated by REX1-high) show limited layer formation potential, implying that a shift away from ground state is necessary for self-organized layer formation on the mesh substrates.

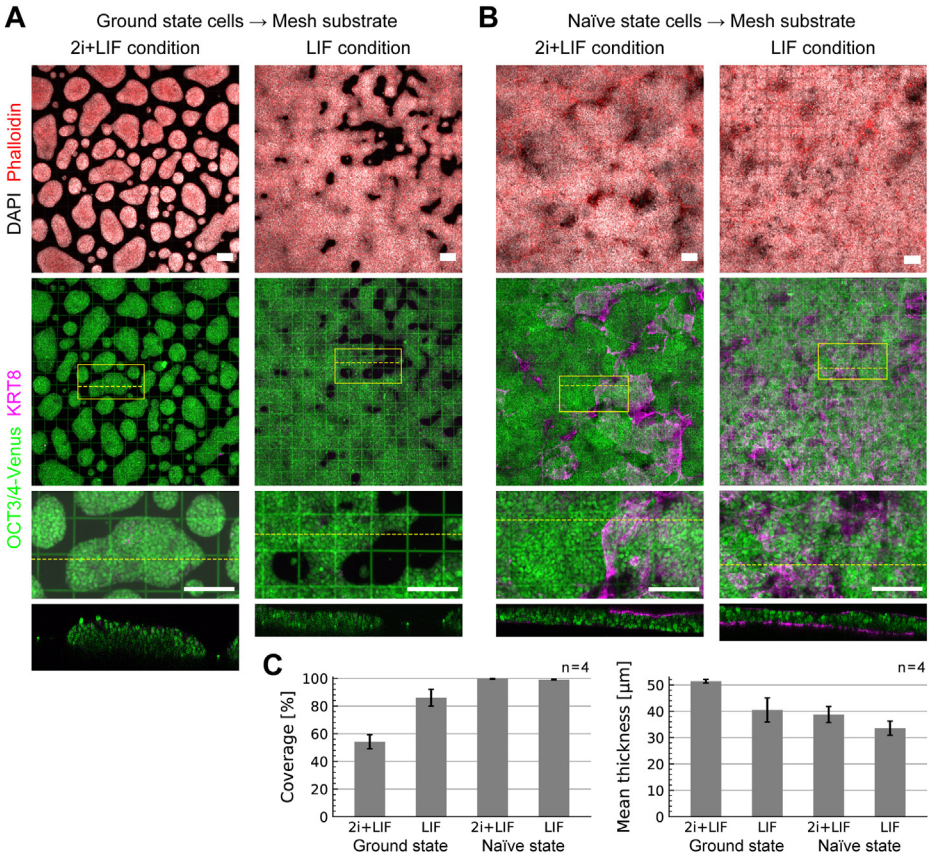

Fig. 2. Layer formation assays for the ground and naïve state cells on mesh substrates. (A) Discontinuous layer formation by the ground state cells on mesh substrates under 2i + LIF and LIF conditions at Day 3. (B) Self-organized layer formation of the naïve state cells on mesh substrates under 2i + LIF and LIF conditions at Day 3. Enlarged views of the yellow boxed region and vertical cross-sections at position of the yellow broken line were shown in bottom panels. (C) Quantitative image analyses for the mesh coverage and mean thickness of each condition. The analyses for coverage and mean thickness were performed using 4 biological samples (4 images each) for each condition. Scale bars: 100 μm. Error bars: mean ± SD.

3.3. Naïve state cells at the sites of mesh closure exhibited pronounced KRT8 meshwork

To observe the process of mesh closure more closely, we focused on KRT8+ cells which were observed to be widely scattered around OCT3/4+ clusters under dish culture (Fig. 1B, right). We performed immunofluorescence microscopy at 6 h, Day 1 and Day 2 to monitor the self-organized layer formation by naïve state mESCs on a mesh substrate under LIF condition (Fig. 4A). At 6 h after seeding, the naïve state cells had successfully adhered on the mesh lines and could be seen starting to fill the mesh openings. At this early stage, a monolayer of cells could be seen self-forming in some parts of the substrate. Also, gaps (holes) were still clearly visible, as confirmed by DAPI and phalloidin staining (Figs. 4A, 6 h). Strikingly, KRT8+ cells were visibly elongated along the mesh lines, and they could be seen surrounding the mesh openings (Figs. 4A, 6 h). By Day 1, the cell layer had increased to a few-cells thick, with KRT8+ cells surrounding patches of OCT3/4+ cells enclaved in the relatively thicker regions of the cell layer (Fig. 4A, Day 1). By Day 2, all the mesh openings had been covered to yield a completely formed cell layer over the initially open meshwork (Fig. 4A, Day 2). Quantitative analyses of the self-organized cell layer formed on the mesh substrate showed that mesh coverage was nearly 100% complete by Day 2, while layer thickness continued to increase to a peak at Day 3 (Fig. 4B). Also, as shown in the enlarged view of Fig. 4C, KRT8+ cells surrounding the closing holes displayed a meshwork of keratin, which appeared to be well-developed than the corresponding F-actin network. Since KRT8+ cells can be regarded as a subpopulation of naïve state mESCs nearly exiting pluripotency [10], the results implicated them in the initiation of cell layer formation on the adhesion-limiting mesh substrates. This was further supported by the observation that most cells around a closing hole exhibited OCT3/4 depletion, which implies loss of pluripotency, as reported in our previous study [20]. Collectively, we postulate that among the naïve state cells, KRT8+ cells could be the main driver of self-organized layer formation by mesh closure, judging from their elongated morphology and pronounced keratin meshwork.

4. Discussion

In this study, we aimed to clarify the contribution of mESCs at different pluripotency states to self-organized layer formation. For this purpose, we examined the layer-forming potential of ground and naïve state mESCs cultured on adhesion-limiting mesh substrates within 3 days. The culture duration was determined based on the findings of our previous study which showed that mESCs could form a continuous layer on the mesh substrates within 3 days [15]. Our results demonstrate that mESCs with ground state-like characteristics, including ground state mESCs and REX1-high population sorted from naïve state mESCs, formed discontinuous cell layers with limited lateral spread within the same culture duration. In contrast, naïve state cells comprising KRT8+ cells succeeded in forming a continuous cell layer by progressive mesh closure.

The fact that the naïve state cells comprising KRT8+ cells were more efficient in layer formation on the mesh substrates suggests that KRT8+ cells could be the main driver of self-organized layer

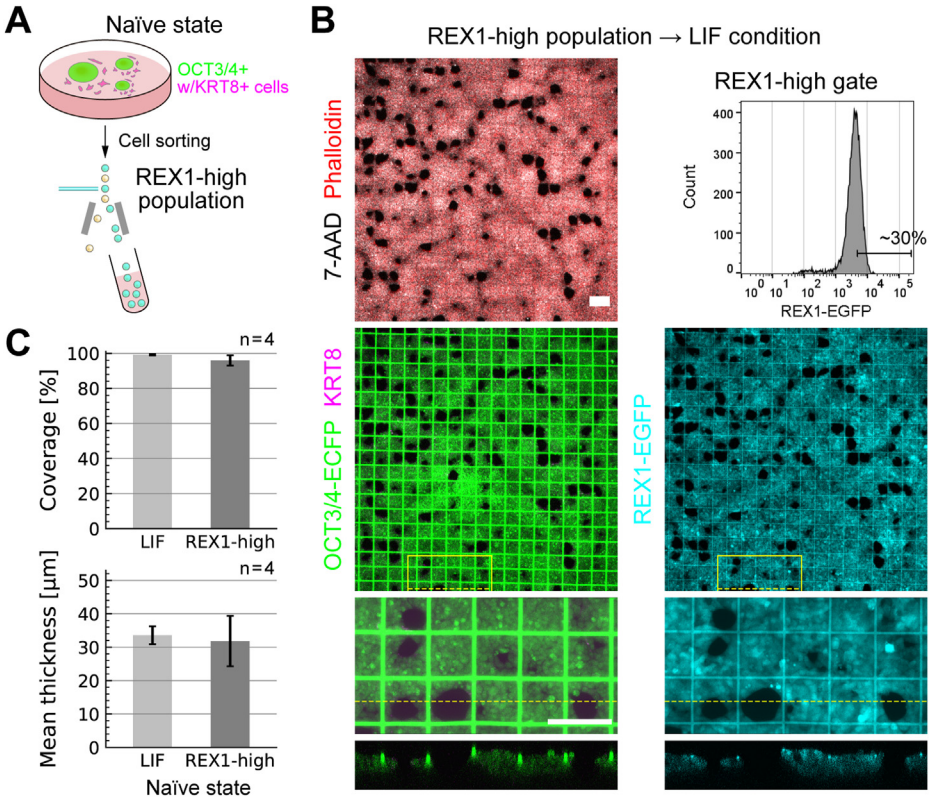

Fig. 3. Discontinuous layer formation by REX1-high population on mesh substrates under LIF conditions at Day 3. (A) Schematic illustration of cell sorting to obtain REX1-high population from a naïve state mESCs. (B) Microscopic images showing discontinuous cell layers formed by REX1-high population at Day 3 under LIF condition. Enlarged views of the yellow boxed region and vertical cross-sections at the position of the yellow broken line are shown in the bottom panels. (C) Quantitative image analyses of mesh coverage and mean thickness for each condition. The analyses of coverage and mean thickness were performed using 4 biological samples (4 images each). Scale bars: 100 μm. Error bars: mean ± SD.

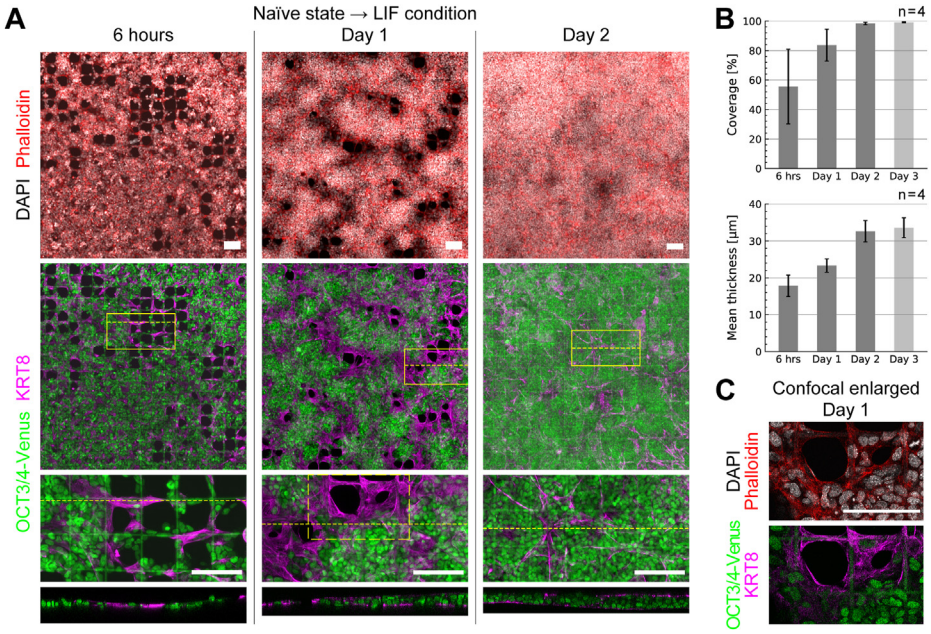

Fig. 4. Self-organized layer formation of the naïve state cells comprising KRT8+ cells on mesh substrates under LIF condition. (A) Microscopic images showing the mesh filling process of self-organized mESC layers on mesh substrates at 6 h, Day 1 and Day 2. Enlarged views of the yellow boxed region and vertical cross-sections at position of the yellow broken line were shown in bottom panels. (B) Quantitative image analyses for the mesh coverage and mean thickness of layers at 6 h, Day 1, Day 2 and Day 3. These analyses were performed using 4 biological samples (4 images each) for each time point. (C) Confocal enlarged views of the yellow dashed-lined boxed region in Fig. 4A, Day 1. Scale bars: 100 μm. Error bars: mean ± SD.

formation by mesh closure, judging from their elongated morphology and pronounced keratin meshwork displayed around closing holes. Indeed, it has been shown that intermediate filaments, which include keratin, provide mechanical support for

active cellular dynamics [21]. Moreover, previous research revealed that KRT8 is an important trigger of inner-outer segmentation and mechanical stabilization during mouse blastocyst morphogenesis [22,23]. Considered in the context of these reports, our results suggest the contribution of KRT8+ cells in self-organized layer formation on adhesion-limiting mesh substrates. Although we could not directly reveal the contribution of KRT8+ cells due to difficulties in sorting for KRT8 knocked-in mESCs, the localization of keratin intermediate filaments during mesh closure could give insight into the mechanism for self-organized layer formation by mESCs *in vitro*.

Conventionally, ground state mESCs are more desirable for differentiation induction to obtain specific lineages due to their homogeneity compared with naïve state mESCs [24]. On the other hand, our study demonstrated that naïve state mESCs comprising KRT8+ cells are more capable of self-organized layer formation compared with relatively more homogeneous mESC populations: ground state mESCs and REX1-high population sorted from naïve state mESCs. Indeed, within the 3-day culture period, the ground state cells formed punctate layers under 2i + LIF condition, indicating their lack of ability to spread laterally by cell-cell adhesion, which is a prerequisite for layer formation on the adhesion-limiting mesh substrates. However, long-term observation would be necessary to confirm how the observed morphology of cell layers by ground state cells under 2i + LIF condition would change, since with extended culture, pluripotency state is bound to change as cells interact with mesh culture environment. Also, it would be important to clarify how the differences in cellular dynamics and gene expression in the heterogeneous naïve state mESCs would contribute to the observed self-organization process. These aspects remain to be investigated fully.

Overall, this study highlights that, compared with ground state mESCs, naïve state mESCs, particularly KRT8+ cells, possess a higher capability to contribute to self-organized layer formation by mesh closure on microengineered scaffolds. The finding that pluripotency state determines the ability of mESCs to form self-organized cell layers on the mesh substrates illustrates an essential aspect that should be considered in scaffold-based tissue engineering with pluripotent stem cells.

Declaration of competing interest

The authors declare that they have no known competing financial interests or personal relationships that could have appeared to influence the work reported in this paper.

Acknowledgements

This research was supported by AMED PRIME under Grant Number 20gm5810023h0004, JSPS KAKENHI Grant Number 20H02594, and partially by the Cooperative Research Program (Joint Usage/Research Center program) of Institute for Frontier Life and Medical Sciences, Kyoto University. We are thankful to lab members, Junko Sunaga and Yoshikiyo Kibe for help with experiments, and Yoshitaka Kameo and Koichiro Maki for useful discussions. We are grateful to the staff of Kyoto University Nano Technology Hub in “Nanotechnology Platform Project” for technical support with the fabrication of mesh substrates used in this study.

References

[1] J. Fu, A. Warmflash, M.P. Lutolf, Stem-cell-based embryo models for fundamental research and translation, Nat. Mater. 20 (2021) 132–144, https://doi.org/10.1038/s41563-020-00829-9.
[2] R. Guo, M. Morimatsu, T. Feng, F. Lan, D. Chang, F. Wan, Y. Ling, Stem cell-derived cell sheet transplantation for heart tissue repair in myocardial infarction, Stem Cell Res. Ther. 11 (2020) 19, https://doi.org/10.1186/s13287-019-1536-y.
[3] T. Takebe, J.M. Wells, Organoids by design, Science 364 (2019) 956–959, https://doi.org/10.1126/science.aaw7567.
[4] L.M. Murrow, R.J. Weber, Z.J. Gartner, Dissecting the stem cell niche with organoid models: an engineering-based approach, Development 144 (2017) 998–1007, https://doi.org/10.1242/dev.140905.
[5] H. Niwa, K. Ogawa, D. Shimosato, K. Adachi, A parallel circuit of LIF signalling pathways maintains pluripotency of mouse ES cells, Nature 460 (2009) 118–122, https://doi.org/10.1038/nature08113.
[6] Y. Toyooka, D. Shimosato, K. Murakami, K. Takahashi, H. Niwa, Identification and characterization of subpopulations in undifferentiated ES cell culture, Development 135 (2008) 909–918, https://doi.org/10.1242/dev.017400.
[7] M.G. Carter, C.A. Stagg, G. Falco, T. Yoshikawa, U.C. Bassey, K. Aiba, L.V. Sharova, N. Shaik, M.S.H. Ko, An in situ hybridization-based screen for heterogeneously expressed genes in mouse ES cells, Gene Expr. Patterns 8 (2008) 181–198, https://doi.org/10.1016/j.gep.2007.10.009.
[8] Q.L. Ying, J. Wray, J. Nichols, L. Batlle-Morera, B. Doble, J. Woodgett, P. Cohen, A. Smith, The ground state of embryonic stem cell self-renewal, Nature 453 (2008) 519–523, https://doi.org/10.1038/nature06968.
[9] G. Guo, L. Pinello, X. Han, S. Lai, L. Shen, T.W. Lin, K. Zou, G.C. Yuan, S.H. Orkin, Serum-based culture conditions provoke gene expression variability in mouse embryonic stem cells as revealed by single-cell analysis, Cell Rep. 14 (2016) 956–965, https://doi.org/10.1016/j.celrep.2015.12.089.
[10] A.A. Kolodziejczyk, J.K. Kim, J.C.H. Tsang, T. Ilicic, J. Henriksson, K.N. Natarajan, A.C. Tuck, X. Gao, M. Bühler, P. Liu, J.C. Marioni, S.A. Teichmann, Single cell RNA-sequencing of pluripotent states unlocks modular transcriptional variation, Cell Stem Cell 17 (2015) 471–485, https://doi.org/10.1016/j.stem.2015.09.011.
[11] D. Papatsenko, H. Darr, I.V. Kulakovskiy, A. Waghray, V.J. Makeev, B.D. MacArthur, I.R. Lemischka, Single-cell analyses of ESCs reveal alternative pluripotent cell states and molecular mechanisms that control self-renewal, Stem Cell Rep 5 (2015) 207–220, https://doi.org/10.1016/j.stemcr.2015.07.004.
[12] R.M. Kumar, P. Cahan, A.K. Shalek, R. Satija, A. DaleyKeyser, H. Li, J. Zhang, K. Pardee, D. Gennert, J.J. Trombetta, T.C. Ferrante, A. Regev, G.Q. Daley, J.J. Collins, Deconstructing transcriptional heterogeneity in pluripotent stem cells, Nature 516 (2014) 56–61, https://doi.org/10.1038/nature13920.
[13] H. Marks, T. Kalkan, R. Menafra, S. Denissov, K. Jones, H. Hofemeister, J. Nichols, A. Kranz, A.F. Stewart, A. Smith, H.G. Stunnenberg, The transcriptional and epigenomic foundations of ground state pluripotency, Cell 149 (2012) 590–604, https://doi.org/10.1016/j.cell.2012.03.026.
[14] C.S. Simon, A.K. Hadjantonakis, C. Schröter, Making lineage decisions with biological noise: lessons from the early mouse embryo, WIREs Dev. Biol. 7 (2018) e319, https://doi.org/10.1002/wdev.319.
[15] Y. Ando, K.O. Okeyo, T. Adachi, Modulation of adhesion microenvironment using mesh substrates triggers self-organization and primordial germ cell-like differentiation in mouse ES cells, APL Bioeng 3 (2019), 016102, https://doi.org/10.1063/1.5072761.
[16] K.O. Okeyo, O. Kurosawa, H. Oana, H. Kotera, M. Washizu, Minimization of cell-substrate interaction using suspended microstructured meshes initiates cell sheet formation by self-assembly organization, Biomed, Phys. Eng. Express 2 (2016), 065019, https://doi.org/10.1088/2057-1976/2/6/065019.
[17] K.O. Okeyo, O. Kurosawa, S. Yamazaki, H. Oana, H. Kotera, H. Nakauchi, M. Washizu, Cell adhesion minimization by a novel mesh culture method mechanically directs trophoblast differentiation and self-assembly organization of human pluripotent stem cells, Tissue Eng. C Methods 21 (2015) 1105–1115, https://doi.org/10.1089/ten.tec.2015.0038.
[18] J. Schindelin, I. Arganda-Carreras, E. Frise, V. Kaynig, M. Longair, T. Pietzsch, S. Preibisch, C. Rueden, S. Saalfeld, B. Schmid, J.Y. Tinevez, D.J. White, V. Hartenstein, K. Eliceiri, P. Tomancak, A. Cardona, Fiji: an open-source platform for biological-image analysis, Nat. Methods 9 (2012) 676–682, https://doi.org/10.1038/nmeth.2019.
[19] N. Schwarz, R. Windoffer, T.M. Magin, R.E. Leube, Dissection of keratin network formation, turnover and reorganization in living murine embryos, Sci. Rep. 5 (2015) 9007, https://doi.org/10.1038/srep09007.
[20] Y. Ando, K.O. Okeyo, J. Sunaga, T. Adachi, Edge-localized alteration in pluripotency state of mouse ES cells forming topography-confined layers on designed mesh substrates, Stem Cell Res. 53 (2021) 102352, https://doi.org/10.1016/j.scr.2021.102352.
[21] P.A. Coulombe, P. Wong, Cytoplasmic intermediate filaments revealed as dynamic and multipurpose scaffolds, Nat. Cell Biol. 8 (2004) 699–706, https://doi.org/10.1038/ncb0804-699.
[22] H.Y.G. Lim, Y.D. Alvarez, M. Gasnier, Y. Wang, P. Tetlak, S. Bissiere, H. Wang, M. Biro, N. Plachta, Keratins are asymmetrically inherited fate determinants in the mammalian embryo, Nature 585 (2020) 404–409, https://doi.org/10.1038/s41586-020-2647-4.
[23] H.Y.G. Lim, N. Plachta, Cytoskeletal control of early mammalian development, Nat. Rev. Mol. Cell Biol. 22 (2021) 548–562, https://doi.org/10.1038/s41580-021-00363-9.
[24] Q.L. Ying, A. Smith, The art of capturing pluripotency: creating the right culture, Stem Cell Rep 8 (2017) 1457–1464, https://doi.org/10.1016/j.stemcr.2017.05.020.